



Nodal line induced large transverse thermoelectric response in the $D0_3$ -type Heusler compound Fe_3Si

Susumu Minami ^{*}, Sota Hogaki, and Takahiro Shimada [†]*Department of Mechanical Engineering and Science, Kyoto University, Nishikyo-ku, Kyoto 615-8540, Japan*

(Received 7 May 2024; accepted 26 June 2024; published 23 July 2024)

Giant magnetic transverse thermoelectric effect, anomalous Nernst effect (ANE), was theoretically and experimentally observed in $3d$ -transition metal compounds. The intrinsic components of ANE can be described from the electronic structure based on the Berry phase concept. The topological electronic structure, such as the Weyl node and nodal lines, induces large Berry curvature, one origin of giant ANE. We investigated transverse thermoelectric properties on ferromagnetic $D0_3$ -type Heusler compounds Fe_3Si based on first-principles calculations. We found large transverse thermoelectric conductivity $\alpha_{xy} \sim 5 \text{ AK}^{-1}\text{m}^{-1}$ is realized with hole carrier doping at room temperature. We also clarified that the nodal line and its stationary point enhance transverse thermoelectric conductivity. These results give us a clue to design high-performance ANE-based magnetic thermoelectric materials.

DOI: [10.1103/PhysRevMaterials.8.075403](https://doi.org/10.1103/PhysRevMaterials.8.075403)

I. INTRODUCTION

The anomalous Nernst effect (ANE), which has a transverse voltage induced by a longitudinal temperature gradient, is attracting renewed interest [1–16]. A charge current in solids \mathbf{J} is given by a temperature gradient ($-\nabla T$) and an external electric field \mathbf{E} as follows: $\mathbf{J} = \hat{\sigma}\mathbf{E} + \hat{\alpha}(-\nabla T)$, where $\hat{\sigma}$ and $\hat{\alpha}$ are the electrical conductivity tensor and thermoelectric (TE) conductivity tensor, respectively. Under an open circuit condition ($\mathbf{J} = 0$), a TE voltage can be described as $\mathbf{E} = \hat{S}(-\nabla T)$; here $\hat{S} \equiv \hat{\alpha}/\hat{\sigma}$ is a TE coefficient. Since breaking the time-reversal symmetry, off-diagonal parts of both tensor $\hat{\sigma}$ and $\hat{\alpha}$ are finite in a magnetic material. Accordingly, the presence of a longitudinal temperature gradient in a magnetic material gives rise to a transverse TE voltage. In essence, ANE represents a TE counterpart of the anomalous Hall effect (AHE) [1–3].

The ANE can be utilized to develop energy-harvesting devices of high efficiency, featuring a straightforward lateral design, exceptional flexibility, and cost-effective production [17,18]. To realize the widespread use of TE devices based on the ANE, a high magnetic transition temperature with no rare and toxic elements is also a crucial condition except for a large ANE signal. Therefore, magnetic $3d$ -transition metal compounds will be a candidate. Indeed, both AHE [4–9,12,13,19–26] and ANE [4,4–9,12,13,27–47] have been observed in numerous $3d$ -transition metal magnetic materials. Especially noteworthy are Co_2MnGa [5,35], iron-based ferromagnets such as fcc- Fe_3X ($X = Al, Ga$) [7] and hexagonal- Fe_3Sn [12], along with $Co_3Sn_2S_2$ [6,24,25,47], which have garnered considerable attention owing to their giant ANE signal and distinctive topological electronic structure near the Fermi energy.

The AHE arises from either extrinsic mechanisms, such as skew-scattering or side-jump [48–50], and intrinsic mechanisms derived from the electronic structure. In terms of the electronic structure, the Berry curvature leads the enhancement of anomalous Hall effect and Nernst effect [1–3]. The recent discovery of topological magnets with a less entangled low-energy electronic structure, such as Weyl or Dirac nodes and nodal lines, is particularly intriguing due to their large anomalous transverse response. In addition, the topological electronic structures hold their robustness from defect, disorder, and roughness [51–53]. Recent experimental studies have reported that the transverse TE responses can be controlled by tuning the Fermi energy through polycrystallization or doping while keeping the ANE derived from the topological electronic structure [9,13,45,47]. Our recent study reported that the density of states composed of topological states such as nodal lines has a crucial role in realizing large transverse transport responses [8], which gives a guiding principle for material design; however, it is still challenging to clarify the topological electronic structure in various magnets.

In this paper, we investigate the transverse TE properties of the $D0_3$ -type Heusler compound Fe_3Si , which has high Curie temperature (820 K [54]), based on the first-principles calculations. The calculated transverse TE conductivity α_{xy} is $1.5 \text{ AK}^{-1}\text{m}^{-1}$ at room temperature, which is consistent with experimental results [44,45]. In addition, α_{xy} reaches $\sim 5 \text{ AK}^{-1}\text{m}^{-1}$ with hole carrier doping. We show a clear correspondence between the nodal line in Fe_3Si and large Berry curvature distribution in the Brillouin zone (BZ). We conclude that the presence of a “Van Hove singularity” in the density of states constituted by the nodal lines (D_{NL}) leads to an enhancement in the transverse TE conductivity α_{xy} .

II. METHODS

The electronic structure of Fe_3Si was obtained by the first-principles calculation based on the density functional

^{*}Contact author: minami.susumu.4f@kyoto-u.ac.jp[†]Contact author: shimada.takahiro.8u@kyoto-u.ac.jp

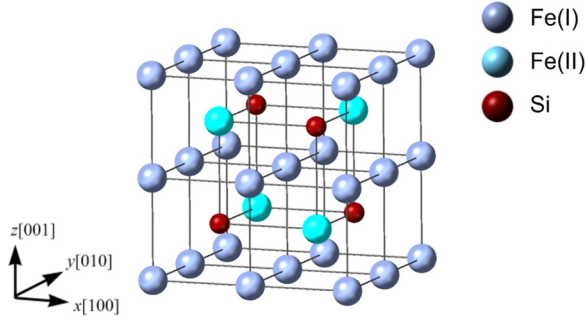


FIG. 1. Crystal structure of the $D0_3$ -type Heusler compound Fe_3Si . Gray, cyan, and red spheres represents Fe(I), Fe(II), and Si atoms, respectively.

theory with the VASP code [55–57]. The crystal structure of $D0_3$ -type Heusler compound Fe_3Si is presented in Fig. 1. $D0_3$ -type Heusler compound Fe_3Si has the symmetry group $Fm\bar{3}m$; Wyckoff positions are characterized by 8c for Fe(I), 4a for Fe(II), and 4b for Si. A plane-wave basis was used to expand the wave function, and the kinetic cutoff energy was set to 700 eV. The effects of the nucleus and electrons were expressed by the projector-augmented wave method [57,58]. We adopted GGA-PBE [59] as the exchange-correlation functional. A k -point sampling of $12 \times 12 \times 12$ with Monkhorst-Pack k -point grid [60], and obtained lattice constant of 5.60 Å, which is consistent with the experimental result [54], were used.

A Wannier function was constructed by the WANNIER90 code [61] from the Bloch states obtained by the first-principles calculation. The Wannier basis was expanded to include (s, d)-character orbitals localized at each Fe site and (s, p)-character orbitals at the Si site, resulting in a total of 44 orbitals per formula unit (f.u.). The intrinsic component of the anomalous Hall conductivity σ_{xy} and the anomalous transverse TE conductivity α_{xy} were obtained by using the Berry curvature formula as

$$\sigma_{xy}(\mu, T) = -\frac{e^2}{\hbar} \int \frac{d\mathbf{k}}{(2\pi)^3} \Omega_{n,z}(\mathbf{k}) f_{n,\mathbf{k}}, \quad (1)$$

$$\alpha_{xy}(\mu, T) = -\frac{1}{e} \int d\varepsilon \sigma_{xy}(\varepsilon, 0) \frac{\varepsilon - \mu}{T} \left(-\frac{\partial f}{\partial \varepsilon} \right), \quad (2)$$

where ε , μ , \hbar , e , f are the band energy, the chemical potential, the reduced Planck constant, the elementary charge, and the Fermi-Dirac distribution function with band index n and wave vector \mathbf{k} , respectively. The Berry curvature for n th band is calculated as follows:

$$\Omega_{n,l} = -2\varepsilon_{i,j,l} \text{Im} \sum_{n' \neq n} \frac{v_{nm',i}(\mathbf{k}) v_{n'n,j}(\mathbf{k})}{[\varepsilon_{n'}(\mathbf{k}) - \varepsilon_n(\mathbf{k})]^2}, \quad (3)$$

where $v_{nm',i}$ is the matrix elements of the velocity operator. The anomalous Hall conductivity in Eq. (1) and transverse TE conductivity in Eq. (2) were evaluated with a $200 \times 200 \times 200$ k -point sampling.

The Mott relation is obtained using Sommerfeld expansion for Eqs. (1) and (2) in the low temperature

limit [62]:

$$\alpha_{xy}^0(\mu, T) = -\frac{\pi^2 k_B^2 T}{3e} \left(\frac{\partial \sigma_{xy}}{\partial \varepsilon} \right)_{\varepsilon=\mu}, \quad (4)$$

where k_B is the Boltzmann constant. Therefore, the Mott relation is usually valid at sufficiently low temperatures. In many thermoelectric materials, α_{ij} can be explained in Eq. (4) in both the conventional TE effect (Seebeck effect) and ANE [29,30,63–65].

The nodal lines have an energy dispersion in the momentum space because they are one-dimensional objects in the BZ composed of band degenerate points. We calculate the density of states composed of the nodal lines as follows [8]:

$$D_{\text{NL}}(\varepsilon) = \sum_{n,\mathbf{k} \in k_{\text{NL}}} \delta(\varepsilon - \varepsilon_{n\mathbf{k}}), \quad (5)$$

where k_{NL} specifies the nodal lines positions in the momentum space. The previous study pointed out that sharp peaks in D_{NL} , such as the Van Hove singularities, enhance transverse TE conductivities. The nodal lines were evaluated by tracking the degeneracy points in momentum space based on the electronic structure without spin-orbit coupling (SOC).

III. RESULTS AND DISCUSSION

A. Electronic structure of Fe_3Si

First, let us consider the electronic structure and magnetic properties of Fe_3Si . Figure 2 shows the band structure along high-symmetry lines in k space and the density of electronic states (DOS) in Fe_3Si . We can see that the small dispersionless majority band (red colored) around $E \sim E_F - 0.2$ eV along the Γ -X direction [Fig. 2(a)]. Due to the small energy dispersion bands, a large DOS from the majority spin appears around $E \sim E_F - 0.2$ eV [Fig. 2(b)]. The calculated total magnetic moment is $\sim 5.07 \mu_B/\text{f.u.}$ along the [001] direction, which is consistent with previous theoretical studies [66–69]. This value is also close to the experimental results [54,70,71]. Moreover, the atomic magnetic moments of Fe(I) at the 8c site and Fe(II) at the 4a site are 1.29 and $2.51 \mu_B/\text{f.u.}$, respectively. The asymmetry in the magnetic moment arises from the arrangement of Fe atoms between the 4a and 8c sites [66].

B. Transverse thermoelectric conductivity

Next, let us focus on the anomalous Hall conductivity (σ_{xy}) and transverse thermoelectric conductivity (α_{xy}). Figure 3 shows the chemical potential dependence of σ_{xy} and α_{xy} . At room temperature, the values of σ_{xy} and α_{xy} reach about $500 \Omega^{-1}\text{cm}^{-1}$ and $1.5 \text{ AK}^{-1}\text{m}^{-1}$, respectively. These values are in good agreement with the experimental value [44,45].

On the other hand, when we focus below the E_F , we can see that the sharp peak of σ_{xy} appears at $E = E_F - 0.22$ eV, of which the values reach about $1500 \Omega^{-1}\text{cm}^{-1}$ [Fig. 3(a)]. The value of α_{xy} vanishes at $E = E_F - 0.22$ eV; however, the size of α_{xy} increases near the peak of σ_{xy} , and its magnitude reaches about $5 \text{ AK}^{-1}\text{m}^{-1}$ [Fig. 3(b)]. This value is

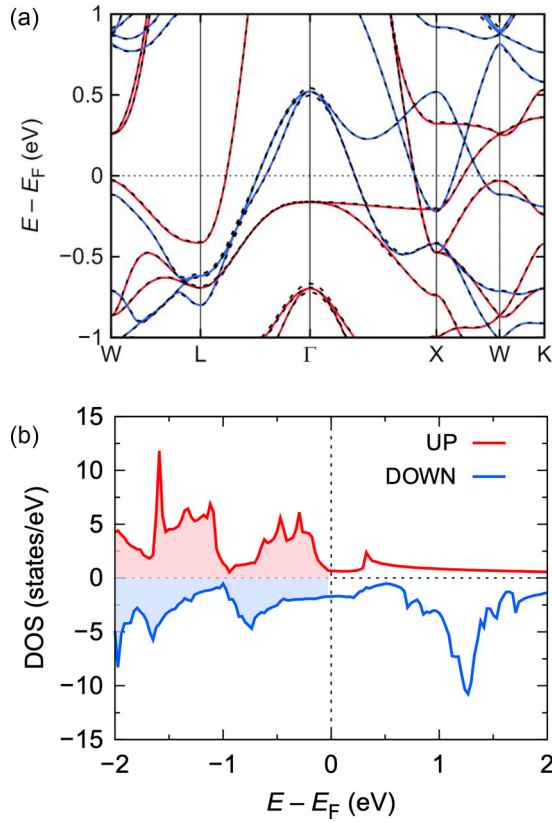


FIG. 2. (a) Band structure along the high-symmetry line and (b) density of states for Fe_3Si . The red and blue lines depict the majority and minority spin bands without SOC, respectively. The dashed black lines represent the band dispersion with SOC.

comparable to those of well-known large ANE materials, such as Co_2MnGa , Mn_3Sn , $\text{Co}_3\text{Sn}_2\text{S}_2$, and Fe_3X ($X = \text{Al}, \text{Ga}, \text{Sn}$), which are topological magnets [4–7,9,12,13]. The sign of α_{xy} indicates the direction of thermoelectric voltage due to ANE, and its magnitude represents the size of ANE. The two peaks with the opposite sign of α_{xy} appear around $E = E_F - 0.22 \text{ eV}$, corresponding to the peak of σ_{xy} . This behavior can be understood as a simple approximation, so-called Mott relation as shown in Eq. (4). The Mott relation gives $\alpha_{xy} \propto \partial\sigma_{xy}/\partial\varepsilon$; in short, the even-functional form of the chemical potential dependence of σ_{xy} leads to the odd-functional form of α_{xy} with two peaks in an opposite sign. According to the recent discovery of the interaction between topological electronic structure and transport phenomenon [4–8,22,24], it is implied that the enhancement of σ_{xy} with a sharp peak and α_{xy} for Fe_3Si originate from the characteristic electronic structure, such as Weyl node, nodal lines.

C. Origin of transverse thermoelectric conductivity

Finally, we discuss the origin of the enhancement of σ_{xy} and α_{xy} in Fe_3Si in terms of the nodal lines and its density of states (D_{NL}). From the Mott relation, α_{xy} also can be rewritten as follows: $\alpha_{xy}(\varepsilon) = \frac{\pi^2}{3} \frac{k_B^2 T}{e} \frac{e^2 T}{h} \sum_{n,k} \Omega_{n,z}(\mathbf{k}) \delta(\varepsilon - \varepsilon_{n,k})$. The origin of the enhancement of α_{xy} is thus attributed to the large

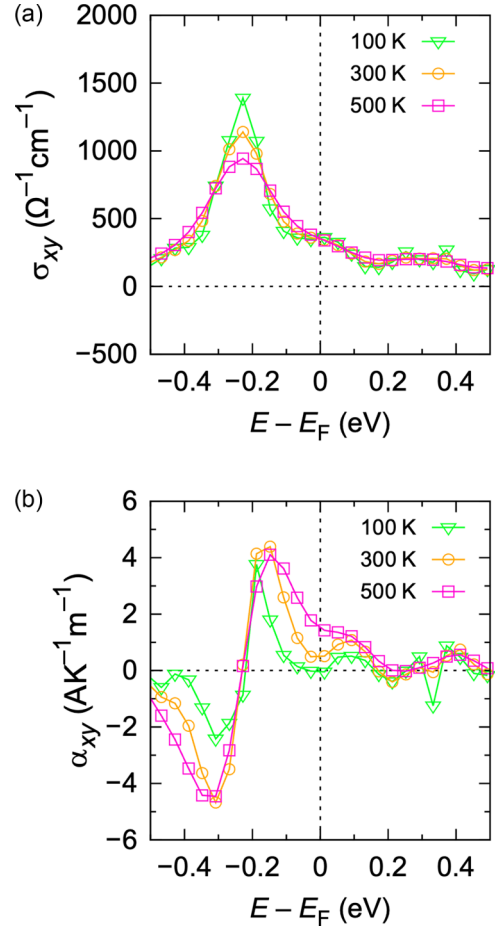


FIG. 3. Chemical potential dependence of (a) anomalous Hall conductivity and (b) transverse thermoelectric conductivity. Triangle, circle, and square line points represent 100 K, 300 K, and 500 K, respectively.

Berry curvature $\Omega_{n,z}(\mathbf{k})$. The previous studies pointed out that a peak of DOS composed of nodal lines (D_{NL}) could prove the enhancement of α_{xy} [8].

To discuss the enhancement of σ_{xy} in terms of D_{NL} , let us clarify the nodal line network in Fe_3Si and the distribution of the large Berry curvature at the peak of σ_{xy} . Figure 4(a) shows the nodal line network and energy dispersion in the BZ. The nodal lines form a ring shape on the $k_i = 0$ plane, and they connect near the X point. For details on evaluating the nodal lines, see the Appendix. Figure 4(b) shows the Berry curvature distribution in the BZ at the peak of σ_{xy} . When comparing Figs. 4(a) and 4(b), we can see the one-to-one correspondence between the nodal line and large Berry curvature contribution.

Moreover, let us confirm the origin of α_{xy} in terms of the divergence from the Mott relation. In the Seebeck effect, the limited conditions, such as singular electronic structures, impurity scattering, and phonon drag, lead to the violation of the Mott relation [72–76]. Similar to ANE, recent studies reported that enhancement of α_{xy} induced by the topological electronic structure breaks the Mott formula; that is, α_{xy}/T shows a logarithmic divergence [5,7–9,12,13,43]. In particular, it

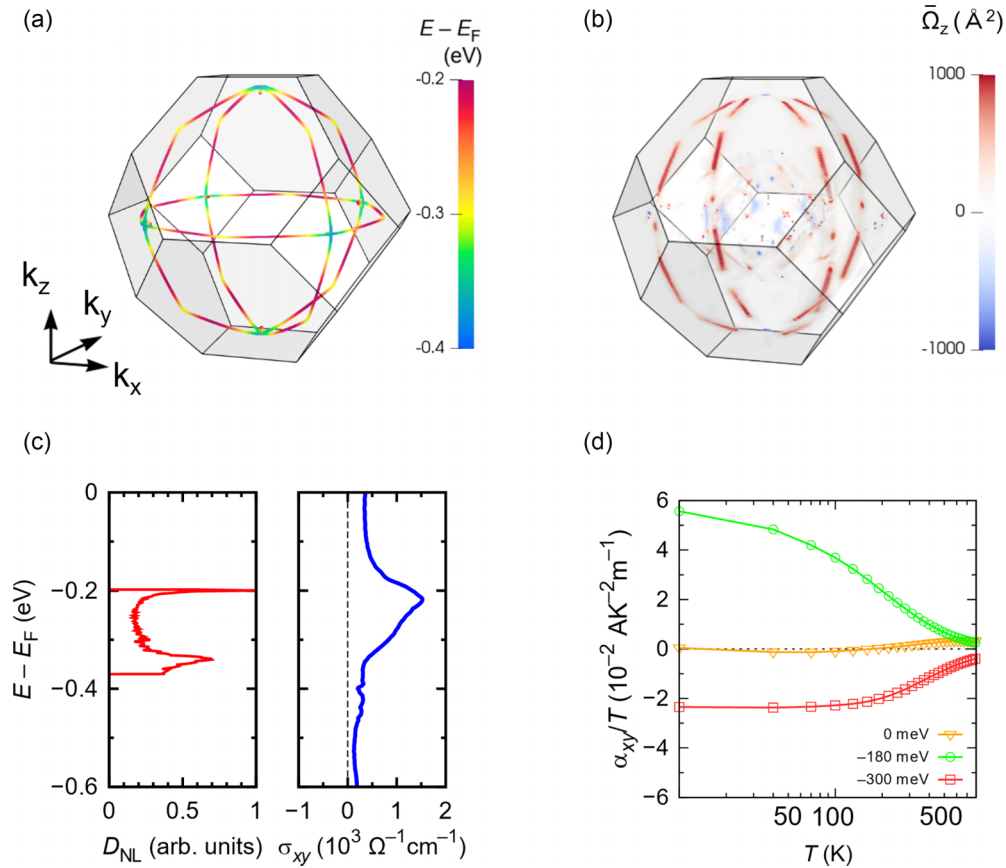


FIG. 4. (a) The nodal line distribution of Fe_3Si in the BZ. The color bar represents the energy range from -0.4 to -0.2 eV. (b) Sum of the Berry curvature over occupied states $\bar{\Omega}_z(\mathbf{k}) \equiv \sum_n \Omega_{n,\mathbf{k}} f(\varepsilon, T = 0)$. Here, we set $\varepsilon = E_F - 0.2$ eV, which corresponds to the peak of σ_{xy} . (c) Chemical potential dependence of D_{NL} for Fe_3Si (left panel) and anomalous Hall conductivity σ_{xy} at $T = 0$ K (right panel). (d) Temperature dependence of α_{xy}/T . Lines with open triangles, open circles, and open squares represent the results for $E = E_F - \mu$; $\mu = 0, -180, -300$ meV, respectively.

theoretically predicted that nodal lines and their stationary points (peak of D_{NL}) lead to large Berry curvature [8].

Figure 4(c) shows the chemical potential dependence σ_{xy} and D_{NL} . Through monitoring energy dispersion in the nodal line, we evaluate D_{NL} [Eq. (5)]. We can see the one-to-one correspondence between the peak of D_{NL} and σ_{xy} at $E \sim E_F - 0.2$ eV. In Fig. 4(d), α_{xy}/T exhibits enhancement and displays a distinctive temperature dependence at $E = E_F - 180, -300$ meV; $\alpha_{xy}/T \sim 0$ at E_F since the σ_{xy} is almost constant with the chemical potential around E_F . On the other hand, α_{xy}/T at $E = E_F - 180, 300$ meV shows the violation of the Mott relation. This indicates that D_{NL} could be a probe to detect the enhancement of σ_{xy} and α_{xy} in Fe_3Si , and its origin is the large D_{NL} and Berry curvature on the nodal line, as shown in Fig. 4(a).

Note that we need to consider the distribution of the nodal line on the momentum space and the magnetization direction to directly connect the peak of D_{NL} and the enhancement of σ_{xy} . There are two D_{NL} peaks at $E \sim E_F - 0.2$ eV and $E \sim E_F - 0.35$ eV, as shown in Fig. 4(c). The lower peak is derived from local minima points for the nodal lines, which are close to the X points near the Brillouin zone boundary, and these

coordinates can be described as $X(\pm k, 0, 0)$, $Y(0, \pm k, 0)$, and $Z(0, 0, \pm k)$. Due to the magnetization direction allying with the [001] direction, only $Z(0, 0, \pm k)$ points work effectively for σ_{xy} and Berry curvature. Indeed, the Berry curvature on the $k_z = 0$ plane seems to vanish [Fig. 4(b)]. For this reason, only the D_{NL} peak at $E \sim E_F - 0.2$ shows clear one-to-one correspondence.

IV. CONCLUSION

In summary, we conducted the first-principles calculation to investigate the origin of AHE and ANE in D0_3 -type Heusler compound Fe_3Si . The transverse TE conductivity α_{xy} reaches $1.5 \text{ AK}^{-1}\text{m}^{-1}$ at room temperature, which agrees well with experimental results [44,45]. Moreover, α_{xy} increases about $5 \text{ AK}^{-1}\text{m}^{-1}$ at room temperature with hole doping. We concluded that the sharp peak of σ_{xy} leads to the enhancement of α_{xy} with hole carrier doping. We also concluded that the large Berry curvature originating from the nodal line could be an origin of the enhancement of AHE and ANE in Fe_3Si , and the DOS composed by nodal lines (D_{NL}) could be a probe for the enhancement transverse TE conductivity α_{xy} . From

the experimental aspect, tuning the peak of D_{NL} in Fe_3Si at the Fermi energy might be realized by controlling electronic structure and exchange splitting via chemical doping or external field due to the featured nodal lines constructed by the majority spins. These present results could provide useful guide principles for designing large ANE materials.

ACKNOWLEDGMENTS

The authors acknowledge financial support from Japan Society for the Promotion of Science (JP) KAKENHI (Grants No. JP22K14587, No. JP23H00159, No. JP23K17720, No. JP24H00032, and No. JP24K00758) and the JST FOREST Program (Grant No. JPMJFR222H). The computations in this research were partially performed using the facilities of the Supercomputer Center, the Institute for Solid State Physics, the University of Tokyo.

APPENDIX: EVALUATING NODAL LINE NETWORK OF Fe_3Si

In order to discuss the DOS composed of nodal lines in Fe_3Si , We evaluate the nodal line network in the BZ by monitoring degenerate bands based on the electronic structure without SOC. Figure 5(a) shows the band structure for Fe_3Si and degenerate points on the high-symmetry line. The nodal line network is constructed with the denoted two majority spin bands, shown in Fig. 5(a). Figure 5(b) shows a three-dimensional band structure on the $k_z = 0$ plane and the nodal line (red line). We can see that the nodal line has energy dispersion, which induces the peak of D_{NL} .

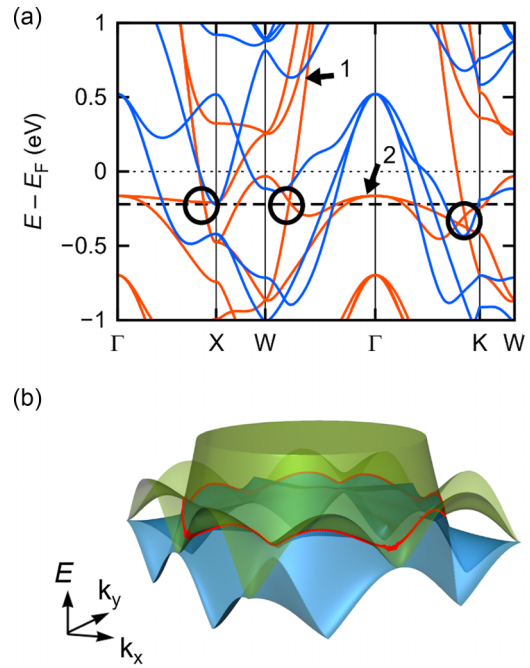


FIG. 5. (a) Band structure of Fe_3Si . Red and blue lines represent the majority and minority spin bands computed without SOC. The denoted majority spin bands 1 and 2 construct the nodal line, and its degenerate points are marked in the black circles. The horizontal dashed black line represents the energy with a peak of σ_{xy} at $E = E_F - 0.2 eV$. (b) Three-dimensional band structure on the $k_z = 0$ plane. Green and blue planes correspond to the majority bands denoted as 1 and 2 in (a), respectively. Red colored ring represents the nodal line on this plane.

[1] D. Xiao, Y. Yao, Z. Fang, and Q. Niu, *Phys. Rev. Lett.* **97**, 026603 (2006).
 [2] N. Nagaosa, J. Sinova, S. Onoda, A. H. MacDonald, and N. P. Ong, *Rev. Mod. Phys.* **82**, 1539 (2010).
 [3] D. Xiao, M.-C. Chang, and Q. Niu, *Rev. Mod. Phys.* **82**, 1959 (2010).
 [4] M. Ikhlas, T. Tomita, T. Koretsune, M.-T. Suzuki, D. Nishio-Hamane, R. Arita, Y. Otani, and S. Nakatsuji, *Nat. Phys.* **13**, 1085 (2017).
 [5] A. Sakai, Y. Mizuta, A. Nugroho, R. Sihombing, T. Koretsune, M. Suzuki, N. Takemori, R. Ishii, D. Nishio-Hamane, R. Arita, P. Goswami, and S. Nakatsuji, *Nat. Phys.* **14**, 1119 (2018).
 [6] S. N. Guin, P. Vir, Y. Zhang, N. Kumar, S. J. Watzman, C. Fu, E. Liu, K. Manna, W. Schnelle, J. Gooth, C. Shekhar, Y. Sun, and C. Felser, *Adv. Mater.* **31**, 1806622 (2019).
 [7] A. Sakai, S. Minami, T. Koretsune, T. Chen, T. Higo, Y. Wang, T. Nomoto, M. Hirayama, S. Miwa, D. Nishio-Hamane, F. Ishii, R. Arita, and S. Nakatsuji, *Nature (London)* **581**, 53 (2020).
 [8] S. Minami, F. Ishii, M. Hirayama, T. Nomoto, T. Koretsune, and R. Arita, *Phys. Rev. B* **102**, 205128 (2020).
 [9] T. Chen, T. Tomita, S. Minami, M. Fu, T. Koretsune, M. Kitatani, I. Muhammad, D. Nishio-Hamane, R. Ishii, F. Ishii, R. Arita, and S. Nakatsuji, *Nat. Commun.* **12**, 572 (2021).
 [10] T. Asaba, V. Ivanov, S. M. Thomas, S. Y. Savrasov, J. D. Thompson, E. D. Bauer, and F. Ronning, *Sci. Adv.* **7**, eabf1467 (2021).
 [11] B. He, C. Şahin, S. R. Boona, B. C. Sales, Y. Pan, C. Felser, M. E. Flatté, and J. P. Heremans, *Joule* **5**, 3057 (2021).
 [12] T. Chen, S. Minami, A. Sakai, Y. Wang, Z. Feng, T. Nomoto, M. Hirayama, R. Ishii, T. Koretsune, R. Arita, and S. Nakatsuji, *Sci. Adv.* **8**, eabk1480 (2022).
 [13] Z. Feng, S. Minami, S. Akamatsu, A. Sakai, T. Chen, D. Nishio-Hamane, and S. Nakatsuji, *Adv. Funct. Mater.* **32**, 2206519 (2022).
 [14] Y. Pan, C. Le, B. He, S. J. Watzman, M. Yao, J. Gooth, J. P. Heremans, Y. Sun, and C. Felser, *Nat. Mater.* **21**, 203 (2022).
 [15] S. Nakatsuji and R. Arita, *Annu. Rev. Condens. Matter Phys.* **13**, 119 (2022).
 [16] M. Ceccardi, A. Zeugner, L. C. Folkers, C. Hess, B. Büchner, D. Marré, A. Isaeva, and F. Caglieris, *npj Quantum Mater.* **8**, 76 (2023).
 [17] Y. Sakuraba, *Scr. Mater.* **111**, 29 (2016).
 [18] M. Mizuguchi and S. Nakatsuji, *Sci. Tech. Adv. Mater.* **20**, 262 (2019).
 [19] T. Jungwirth, Q. Niu, and A. H. MacDonald, *Phys. Rev. Lett.* **88**, 207208 (2002).
 [20] J.-C. Tung and G.-Y. Guo, *New J. Phys.* **15**, 033014 (2013).

- [21] H. Chen, Q. Niu, and A. H. MacDonald, *Phys. Rev. Lett.* **112**, 017205 (2014).
- [22] S. Nakatsuji, N. Kiyohara, and T. Higo, *Nature (London)* **527**, 212 (2015).
- [23] N. Kiyohara, T. Tomita, and S. Nakatsuji, *Phys. Rev. Appl.* **5**, 064009 (2016).
- [24] E. Liu, Y. Sun, N. Kumar, L. Muechler, A. Sun, L. Jiao, S.-Y. Yang, D. Liu, A. Liang, Q. Xu, J. Kroder, V. Süß, H. Borrmann, C. Shekhar, Z. Wang, C. Xi, W. Wang, W. Schnelle, S. Wirth, Y. Chen *et al.*, *Nat. Phys.* **14**, 1125 (2018).
- [25] M. Tanaka, Y. Fujishiro, M. Mogi, Y. Kaneko, T. Yokosawa, N. Kanazawa, S. Minami, T. Koretsune, R. Arita, S. Tarucha, M. Yamamoto, and Y. Tokura, *Nano Lett.* **20**, 7476 (2020).
- [26] K. Manna, L. Muechler, T.-H. Kao, R. Stinshoff, Y. Zhang, J. Gooth, N. Kumar, G. Kreiner, K. Koepf, R. Car, J. Kübler, G. H. Fecher, C. Shekhar, Y. Sun, and C. Felser, *Phys. Rev. X* **8**, 041045 (2018).
- [27] A. W. Smith, *Phys. Rev. (Series I)* **33**, 295 (1911).
- [28] W.-L. Lee, S. Watauchi, V. L. Miller, R. J. Cava, and N. P. Ong, *Phys. Rev. Lett.* **93**, 226601 (2004).
- [29] T. Miyasato, N. Abe, T. Fujii, A. Asamitsu, S. Onoda, Y. Onose, N. Nagaosa, and Y. Tokura, *Phys. Rev. Lett.* **99**, 086602 (2007).
- [30] Y. Pu, D. Chiba, F. Matsukura, H. Ohno, and J. Shi, *Phys. Rev. Lett.* **101**, 117208 (2008).
- [31] Y. Sakuraba, K. Hasegawa, M. Mizuguchi, T. Kubota, S. Mizukami, T. Miyazaki, and K. Takanashi, *Appl. Phys. Express* **6**, 033003 (2013).
- [32] K. Hasegawa, M. Mizuguchi, Y. Sakuraba, T. Kamada, T. Kojima, T. Kubota, S. Mizukami, T. Miyazaki, and K. Takanashi, *Appl. Phys. Lett.* **106**, 252405 (2015).
- [33] G.-Y. Guo and T.-C. Wang, *Phys. Rev. B* **96**, 224415 (2017).
- [34] S. Minami, F. Ishii, Y. P. Mizuta, and M. Saito, *Appl. Phys. Lett.* **113**, 032403 (2018).
- [35] S. N. Guin, K. Manna, J. Noky, S. J. Watzman, C. Fu, N. Kumar, W. Schnelle, C. Shekhar, Y. Sun, J. Gooth, and C. Felser, *NPG Asia Mater.* **11**, 16 (2019).
- [36] J. Xu, W. A. Phelan, and C.-L. Chien, *Nano Lett.* **19**, 8250 (2019).
- [37] J. Noky, Q. Xu, C. Felser, and Y. Sun, *Phys. Rev. B* **99**, 165117 (2019).
- [38] H. Nakayama, K. Masuda, J. Wang, A. Miura, K.-I. Uchida, M. Murata, and Y. Sakuraba, *Phys. Rev. Mater.* **3**, 114412 (2019).
- [39] Z. Shi, S.-J. Xu, L. Ma, S.-M. Zhou, and G.-Y. Guo, *Phys. Rev. Appl.* **13**, 054044 (2020).
- [40] R. Syariati, S. Minami, H. Sawahata, and F. Ishii, *APL Mater.* **8**, 041105 (2020).
- [41] A. Miura, K. Masuda, T. Hirai, R. Iguchi, T. Seki, Y. Miura, H. Tsuchiura, K. Takanashi, and K.-I. Uchida, *Appl. Phys. Lett.* **117**, 082408 (2020).
- [42] D. Khadka, T. R. Thapaliya, S. Hurtado Parra, J. Wen, R. Need, J. M. Kikkawa, and S. X. Huang, *Phys. Rev. Mater.* **4**, 084203 (2020).
- [43] H. Nakamura, S. Minami, T. Tomita, A. A. Nugroho, and S. Nakatsuji, *Phys. Rev. B* **104**, L161114 (2021).
- [44] Y. Hamada, Y. Kurokawa, T. Yamauchi, H. Hanamoto, and H. Yuasa, *Appl. Phys. Lett.* **119**, 152404 (2021).
- [45] Y. Wang, S. Minami, A. Sakai, T. Chen, Z. Feng, D. Nishio-Hamane, and S. Nakatsuji, [arXiv:2405.01800](https://arxiv.org/abs/2405.01800).
- [46] G. Xing, K. Masuda, T. Tadano, and Y. Miura, *Acta Mater.* **270**, 119856 (2024).
- [47] S. Noguchi, K. Fujiwara, Y. Yanagi, M.-T. Suzuki, T. Hirai, T. Seki, K.-i. Uchida, and A. Tsukazaki, *Nat. Phys.* **20**, 254 (2024).
- [48] J. Smit, *Physica* **21**, 877 (1955).
- [49] J. Smit, *Physica* **24**, 39 (1958).
- [50] L. Berger, *Phys. Rev. B* **2**, 4559 (1970).
- [51] C. Chen, S. He, H. Weng, W. Zhang, L. Zhao, H. Liu, X. Jia, D. Mou, S. Liu, J. He, Y. Peng, Y. Feng, Z. Xie, G. Liu, X. Dong, J. Zhang, X. Wang, Q. Peng, Z. Wang, S. Zhang *et al.*, *Proc. Natl. Acad. Sci. USA* **109**, 3694 (2012).
- [52] G. Chang, S.-Y. Xu, D. S. Sanchez, S.-M. Huang, C.-C. Lee, T.-R. Chang, G. Bian, H. Zheng, I. Belopolski, N. Alidoust, H.-T. Jeng, A. Bansil, H. Lin, and M. Z. Hasan, *Sci. Adv.* **2**, e1600295 (2016).
- [53] A. Bandyopadhyay, S. Datta, D. Jana, S. Nath, and M. M. Uddin, *Sci. Rep.* **10**, 2502 (2020).
- [54] Y. Nishino, S.-Y. Inoue, S. Asano, and N. Kawamiya, *Phys. Rev. B* **48**, 13607 (1993).
- [55] G. Kresse and J. Furthmüller, *Comput. Mater. Sci.* **6**, 15 (1996).
- [56] G. Kresse and J. Furthmüller, *Phys. Rev. B* **54**, 11169 (1996).
- [57] G. Kresse and D. Joubert, *Phys. Rev. B* **59**, 1758 (1999).
- [58] P. E. Blöchl, *Phys. Rev. B* **50**, 17953 (1994).
- [59] J. P. Perdew, M. Ernzerhof, and K. Burke, *J. Chem. Phys.* **105**, 9982 (1996).
- [60] H. J. Monkhorst and J. D. Pack, *Phys. Rev. B* **13**, 5188 (1976).
- [61] G. Pizzi, V. Vitale, R. Arita, S. Blügel, F. Freimuth, G. Géranton, M. Gibertini, D. Gresch, C. Johnson, T. Koretsune, J. Ibañez-Azpiroz, H. Lee, J.-M. Lihm, D. Marchand, A. Marrazzo, Y. Mokrousov, J. I. Mustafa, Y. Nohara, Y. Nomura, and L. Paulatto, *J. Phys.: Condens. Matter* **32**, 165902 (2020).
- [62] N. Mott and H. Jones, *The Theory of the Properties of Metals and Alloys*, Dover Books on Physics (Dover, New York, 1958).
- [63] M. Cutler and N. F. Mott, *Phys. Rev.* **181**, 1336 (1969).
- [64] M. Jonson and G. D. Mahan, *Phys. Rev. B* **21**, 4223 (1980).
- [65] D. M. Rowe, *Materials, Preparation, and Characterization in Thermoelectrics* (Taylor & Francis, CRC Press, Boca Raton, 2012).
- [66] A. Go, M. Pugaczowa-Michalska, and L. Dobrzyński, *Eur. Phys. J. B* **59**, 1 (2007).
- [67] D. Odkhuu and S. C. Hong, *IEEE Trans. Magn.* **47**, 2920 (2011).
- [68] R. Ma, Q. Xie, J. Huang, W. Yan, and X. Guo, *J. Alloys Compd.* **552**, 324 (2013).
- [69] I. Sandalov, N. Zamkova, V. Zhandun, I. Tarasov, S. Varnakov, I. Yakovlev, L. Solovyov, and S. Ovchinnikov, *Phys. Rev. B* **92**, 205129 (2015).
- [70] A. Paoletti and L. Passari, *Nuovo Cim.* **32**, 25 (1964).
- [71] W. A. Hines, A. H. Menotti, J. I. Budnick, T. J. Burch, T. Litrenta, V. Niculescu, and K. Raj, *Phys. Rev. B* **13**, 4060 (1976).
- [72] J. M. Buhmann and M. Sigrist, *Phys. Rev. B* **88**, 115128 (2013).
- [73] C. Xiao, D. Li, and Z. Ma, *Phys. Rev. B* **93**, 075150 (2016).
- [74] F. Ghahari, H.-Y. Xie, T. Taniguchi, K. Watanabe, M. S. Foster, and P. Kim, *Phys. Rev. Lett.* **116**, 136802 (2016).
- [75] T. Izawa, K. Takashima, S. Konabe, and T. Yamamoto, *Synth. Met.* **225**, 98 (2017).
- [76] M. Ogata and H. Fukuyama, *J. Phys. Soc. Jpn.* **88**, 074703 (2019).